



Review

The Synthesis and Properties of TIPA-Dominated Porous Metal-Organic Frameworks

Hongru Fu ^{1,2}, **Yuying Jiang** ², **Fei Wang** ^{1,*} and **Jian Zhang** ^{1,*}¹ State Key Laboratory of Structural Chemistry, Fujian Institute of Research on the Structure of Matter, Chinese Academy of Sciences, Fuzhou 350002, China; hongrufu2015@163.com² College of Chemistry and Chemical Engineering, Luoyang Normal University, Luoyang 471934, China; jiangyuyinghx@126.com

* Correspondence: wangfei04@fjirsm.ac.cn (F.W.); zhj@fjirsm.ac.cn (J.Z.)

Abstract: Metal-Organic Frameworks (MOFs) as a class of crystalline materials are constructed using metal nodes and organic spacers. Polydentate N-donor ligands play a mainstay-type role in the construction of metal–organic frameworks, especially cationic MOFs. Highly stable cationic MOFs with high porosity and open channels exhibit distinct advantages, they can act as a powerful ion exchange platform for the capture of toxic heavy-metal oxoanions through a Single-Crystal to Single-Crystal (SC-SC) pattern. Porous luminescent MOFs can act as nano-sized containers to encapsulate guest emitters and construct multi-emitter materials for chemical sensing. This feature article reviews the synthesis and application of porous Metal-Organic Frameworks based on tridentate ligand tris (4-(1H-imidazol-1-yl) phenyl) amine (TIPA) and focuses on design strategies for the synthesis of TIPA-dominated Metal-Organic Frameworks with high porosity and stability. The design strategies are integrated into four types: small organic molecule as auxiliaries, inorganic oxyanion as auxiliaries, small organic molecule as secondary linkers, and metal clusters as nodes. The applications of ratiometric sensing, the adsorption of oxyanions contaminants from water, and small molecule gas storage are summarized. We hope to provide experience and inspiration in the design and construction of highly porous MOFs base on polydentate N-donor ligands.



Citation: Fu, H.; Jiang, Y.; Wang, F.; Zhang, J. The Synthesis and Properties of TIPA-Dominated Porous Metal-Organic Frameworks. *Nanomaterials* **2021**, *11*, 2791. <https://doi.org/10.3390/nano1112791>

Academic Editor: Ullrich Scherf

Received: 26 September 2021

Accepted: 18 October 2021

Published: 21 October 2021

Publisher's Note: MDPI stays neutral with regard to jurisdictional claims in published maps and institutional affiliations.



Copyright: © 2021 by the authors. Licensee MDPI, Basel, Switzerland. This article is an open access article distributed under the terms and conditions of the Creative Commons Attribution (CC BY) license (<https://creativecommons.org/licenses/by/4.0/>).

1. Introduction

Metal-Organic Frameworks (MOFs) are highly crystallized organic-inorganic hybrid materials that are formed through self-assembly of metal ions/metal clusters and organic ligands [1]. MOFs have strong structural advantages and benefit from a predesigned architecture, well-ordered porous structures, and versatile building blocks, which enable them to be sculpted into desirable materials for diverse applications [2–9].

Luminescent Metal-Organic Frameworks (LMOFs), a subclass of MOFs, are promising light-harvesting and energy transfer platforms that have been widely explored in single-phased white-light emission, optical sensors, photocatalysis, and anticounterfeiting applications [10–18]. MOFs have multiple photonic units, originating from inorganic metal nodes, organic chromophores, or synergistic effects of host-guest compositions. Importantly, highly porous MOFs can serve as nanocontainers to encapsulate guest emitters. Especially, benefiting from confinement and dispersion effects, the introduction of organic fluorescent dyes into MOFs can remarkably minimize nonradiative processes and Aggregation-Caused Quenching (ACQ) effects, and greatly enhanced the luminescent quantum yields [19–22]. Making full use of the encapsulation of organic luminophores and dyes, multiple emission host-guest systems can be easily prepared, which is crucial to achieve a tunable emission that contributes to ratiometric fluorescence sensing.

Cationic MOFs featuring high porosity and water stability have been demonstrated as exceptional ion-exchange platforms for the capture of toxic oxoanions and dyes. Importantly, compared with other solid porous materials, such as zeolites, activated carbons, and molecular sieves, ion exchange can be achieved via Single-Crystal to Single-Crystal (SC-SC) transformations [20–29], consequently leading to the obtaining of accurate host-guest structures to directly determine host-guest interactions and adsorption behaviors, as well as providing a new approach to reveal adsorption mechanisms.

We narrowed our interest in MOFs based on tris (4-(1H-imidazol-1-yl)phenyl) amine (TIPA), and exploited its fascinating structures and properties. Triphenylamine (TPA) has a rigid aromatic moiety and electron-donor unit, featuring two-photon absorption [30], outstanding hole mobility [31], high optical stability [32], and high molar extinction coefficient [33], and exhibits intrinsically excellent photophysical and chemical characteristics (Figure 1). Electron-withdrawing substituents, such as imidazole on the ligand, can finely modulate optical property by forming a push–pull structure with the electron-rich triphenylamine core. In addition, TIPA, as a relatively long and semi-rigid star-like structure, more easily meets the geometric requirements of metal ions. Given these facts, porous MOFs with open windows can be constructed using TIPA as the linker. Furthermore, based on the strategy of charge balance and compensation, cationic MOFs consisting of nanoscale channels can be built through the assembly of metal centers and TIPA molecules, which allows to trap toxic oxoanions. In addition, luminescent MOFs or guest-encapsulated MOFs can be prepared for fluorescence sensors. As a result, TIPA can play a significant role in crystal chemistry and coordination chemistry, further promoting the structural and functional diversity of MOFs.

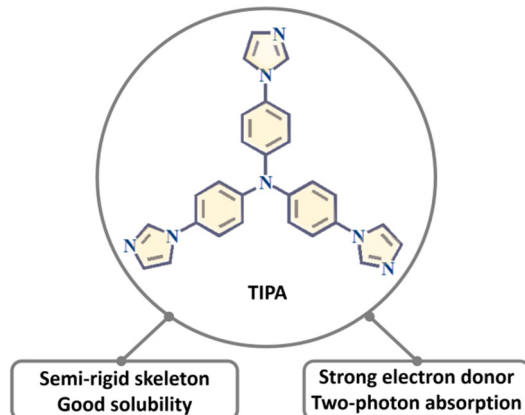


Figure 1. The skeleton and optical properties of TIPA.

In this article, we mainly focus on the synthesis and application of the highly porous MOF base with TIPA ligands. We sum up synthesis strategies for MOFs with high pores, including small organic molecule as auxiliaries, inorganic oxyanion as auxiliaries, small organic molecule as secondary linkers, and metal clusters as nodes, as well as discuss crucial factors. We also introduce some applications of highly porous frameworks, such as the capture of toxic oxoanions, luminescent detection, and the adsorption and separation of small-molecule gases. In particular, we highlight the advantage of TIPA-based MOFs as Single-Crystal containers for the encapsulation of toxic oxoanions and small molecule dyes using the SC-SC pattern. In addition, the prospect of future research in this field and the still-existing challenges are also discussed.

2. Construction Strategies for TIPA-Dominated Porous MOFs

The preparation of a highly porous Metal-Organic Framework is quite a complicated process and is associated with crystallization environments. More precisely, many factors, such as the organic ligands, metal ions, temperature, pH value, and the molar ratio of raw materials, can affect the formation of MOFs [34–39]. To a certain extent, organic ligands

and metal nodes play a central role. TIPA, as a semi-rigid tridentate neutral ligand, has a relatively long skeleton, providing the prerequisite to construct a highly porous framework.

In the literature, using TIPA molecules as linkers for the synthesis of MOFs has been reported since 2011 [40]. The corresponding compounds were summarized in Table 1. Hundreds of TIPA-dominated MOFs have been synthesized, mainly by adopting the strategy of the mixing the ligands of TIPA molecules and various carboxylate ligands in early stages. As a whole, the great accomplishments exhibited these contributions to the construction and evolution of topological structures, especially, the fascinating polyrotaxane, polycatenation, and high-fold interpenetrating structures, have been created [41–59]. Nevertheless, frameworks that are highly porous and with open channels are exceedingly rare, and their properties were only focused on luminescence spectroscopy; the application and function was not developed. Until 2014, we explored a new way to promote crystal coordination chemistry of TIPA, we tried to synthesize cationic porous MOFs only using TIPA molecules as linkers, without the assistance of carboxylate ligands [60]. We took the strategy one step further, and expanded to other special routes, resulting in the realization of rigid and porous frameworks. A milestone work was reported by our group in 2015, namely, a water stable MOF FIR-53 that exhibited fast capture of $\text{Cr}_2\text{O}_7^{2-}$ ions through the SC-SC approach [61]. Subsequently, dozens of TIPA-dominated MOFs with high stability and porosity were successfully prepared. Thus far, the design strategies of highly porous MOFs based on TIPA have been exploited and can be classified into four major categories: (1) small organic molecule as auxiliaries, (2) inorganic oxyanion as auxiliaries, (3) small organic molecule as secondary linkers, and (4) metal cluster as nodes.

Table 1. Examples of MOFs based on TIPA.

MOF	Dimension	Porosity	Auxiliary Ligand	Ref.
$[\text{Cd}(\text{TIPA})(\text{NO}_3)_2 \cdot 5\text{H}_2\text{O}]_n$	2D	28.7%		
$[\text{Co}(\text{TIPA})_{1/3} \cdot \text{Cl}_3 \cdot 2\text{H}_2\text{O}]_n$	2D	52.8%		[40]
$[\text{Co}(\text{TIPA}) \cdot (\text{5-OH-bdc})_3 \cdot 2\text{H}_2\text{O}]_n$	2D	none		
$[\text{Cd}_2(\text{TIPA})_2 \cdot (\text{5-OHbdc})_2 \cdot 5.5\text{H}_2\text{O}]_n$	3D	34.4%		
$[\text{Ag}_{0.52}\text{Na}_{0.48}(\beta\text{-Mo}_8\text{O}_{26}) (\text{H}_2\text{O})] [\text{Ag}_3(\text{Tipa})_2]$	3D	none		[41]
$[\text{Ag}_8(\text{Tipa})_4(\beta\text{-Mo}_8\text{O}_{26})] [\text{H}_2(\beta\text{-Mo}_8\text{O}_{26})] 5\text{H}_2\text{O}$	2D	none		[42]
$[\text{Ag}_3(\text{OH})(\text{H}_2\text{O})_2(\text{Tipa})_{2.5}] [\text{Mo}_2\text{O}_7]_3 \cdot 4.5\text{H}_2\text{O}$	3D	none		
$[\text{Cd}(\text{Tipa})(\text{L}1)_2] \text{H}_2\text{O}$	2D	none		
$[\text{Cd}(\text{Tipa})(\text{L}2)] \text{H}_2\text{O}$	2D	none		
$[\text{Cd}(\text{Tipa})(\text{L}2)] \text{CH}_3\text{OH} \cdot \text{H}_2\text{O}$	3D	none		
$[\text{Cd}(\text{Tipa})(\text{L}3)] (\text{H}_2\text{O})$	3D	none		
$[\text{Mn}(\text{Tipa})(\text{L}2)] \text{H}_2\text{O}$	2D	none		
$[\text{Ni}_2(\text{Tipa})_2(\text{L}4)] (\text{H}_2\text{O})_2 \cdot 2\text{Cl}_4 \cdot 4\text{H}_2\text{O}$	2D	none		
$[\text{Ni}_2(\text{Tipa})_2(\text{L}5) (\text{H}_2\text{O})_4] (\text{H}_2\text{L}5) 0.5\text{H}_2\text{O}$	2D	none		
$[[\text{Zn}(\text{TIPA})(\text{mal})_{1/2}] (\text{NO}_3)_3 \cdot 3\text{H}_2\text{O}]_n$	3D	41.9%		
$[[\text{Zn}(\text{TIPA})(\text{glu})_{1/2}] (\text{NO}_3)_3 \cdot \text{H}_2\text{O}]_n$	3D	27.2%		
$\{[\text{Co}(\text{TIPA})(\text{trans-chdc}) (\text{H}_2\text{O})]\cdot \text{H}_2\text{O}\}_n$	2D	none		
$\{[\text{Ni}(\text{TIPA})(\text{trans-chdc}) (\text{H}_2\text{O})]\cdot \text{H}_2\text{O}\}_n$	2D	none		
$\{[\text{Co}(\text{TIPA})(\text{seb})_{1/2}] (\text{NO}_3)_3 \cdot \text{H}_2\text{O}\}_n$	2D	none		
$\{[\text{Ni}(\text{TIPA})(\text{seb})_{1/27}] (\text{NO}_3)_3 \cdot \text{H}_2\text{O}\}_n$	2D	none		
$\{[\text{Zn}_2(\text{TIPA})(\text{btc})(\mu 2\text{-OH})]\cdot 4\text{H}_2\text{O}\}_n$	2D	none		
$\{[\text{Cd}(\text{TPPA})(\text{trans-chdc})]\}_n$	3D	none		
$\{[\text{Co}(\text{TPPA})_2(\text{D-ca})_2]\cdot (\text{H}_2\text{O})\}_n$	2D	none		
$\{[\text{Ni}(\text{TPPA})(\text{btc})(\text{H}_2\text{O})]\cdot (\text{H}_2\text{O})_4\}_n$	3D	none		
$\{[\text{Ni}(\text{TPPA})(\text{trans-chdc})(\text{H}_2\text{O})]\cdot (\text{H}_2\text{O})_4\}_n$	3D	none		
$[\text{Co}_2(\text{TPPA})_2(1,3\text{-bdc})_2 (\text{H}_2\text{O})]_n$	2D	none		
$[\text{Zn}(\text{TPPA})_2(1,3\text{-bdc})]_n$	2D	none		
$[\text{Zn}_6(\text{TPPA})_2(\text{btc})(\text{Hbetc})_2(\text{H}_2\text{betc}) (\text{H}_2\text{O})_6 \cdot 7\text{H}_2\text{O} \cdot 2\text{DMA}]_n$	3D	24.2%	$\text{betc} = 1,2,4,5\text{-benzenetetracarboxylic dianhydride}$	[47]
$[\text{Cu}(\text{TPPA})(\text{NO}_3)_2 (\text{H}_2\text{O})] \cdot 2\text{H}_2\text{O}]_n$	2D	none		
$[\text{Cd}(\text{DIMPPA})(5\text{-OH-bdc})] (\text{H}_2\text{O})_n$	2D	none		
$[\text{Co}(\text{DIMPPA})(5\text{-OH-bdc})] (\text{H}_2\text{O})_n$	2D	none		
$\{[\text{Cd}_2(\text{MIDPPA})_2(\text{D-ca})_2 (\text{H}_2\text{O})_2]\cdot (\text{H}_2\text{O})_5\}_n$	3D	none		
$\{[\text{Co}_{1.5}(\text{TPPA})(\text{BTC}) (\text{H}_2\text{O})_2\cdot 13\text{H}_2\text{O}\}_n$	3D	51%		
$[\text{Co}(\text{TPPA})(\text{PA})]_n$	3D	none		
$[\text{Co}(\text{TPPA})(\text{BDA})_{0.5}(\text{NO}_3)_3 \cdot 3\text{H}_2\text{O}]_n$	3D	27.2%		
$\{[\text{Co}_2(\text{TPPA})_3(\text{OBA})_2 (\text{H}_2\text{O})_3\cdot 2\text{CH}_3\text{CN} \cdot 4\text{H}_2\text{O}\}_n$	2D	none		
$[\{[\text{Co}(\text{TPPA})(\text{AIP}) (\text{H}_2\text{O})\cdot 2\text{H}_2\text{O}\}]_n$	2D	none		
$[\{[\text{Co}(\text{TPPA})(\text{MIP}) (\text{H}_2\text{O})\cdot 2\text{H}_2\text{O}\}]_n$	2D	none		
			$\text{D-H}_2\text{ca} = \text{D-camphor acid}$ $\text{H}_2\text{bdc} = \text{benzene-p-dicarboxylic acid}$ $1,3\text{-H}_2\text{bdc} = 1,3\text{-benzeneddicarboxylic acid}$ $\text{H}_3\text{btc} = 1,3,5\text{-benzenetricarboxylic acid}$ $\text{trans-H}_2\text{chdc} = \text{trans-1,4-cyclohexanedicarboxylic acid}$ $\text{H}_2\text{seb} = \text{sebacic acid}$ $\text{D-H}_2\text{ca} = \text{D-camphor acid}$ $\text{H}_2\text{bdc} = \text{benzene-p-dicarboxylic acid}$ $1,3\text{-H}_2\text{bdc} = 1,3\text{-benzeneddicarboxylic acid}$ $\text{H}_3\text{btc} = 1,3,5\text{-benzenetricarboxylic acid}$ $\text{trans-H}_2\text{chdc} = \text{trans-1,4-cyclohexanedicarboxylic acid}$ $\text{H}_2\text{BDA} = (1,1'\text{-biphenyl})\text{-4,4'-dicarboxylic acid}$ $\text{H}_2\text{OBA} = 4,4'\text{-oxydibenzzoic acid}$ $\text{H}_2\text{AIP} = 5\text{-aminoisophthalic acid}$ $\text{H}_2\text{MIP} = 5\text{-methylisophthalic acid}$	[44] [45] [46] [47] [48] [49] [50] [51] [52]

Table 1. Cont.

MOF	Dimension	Porosity	Auxiliary Ligand	Ref.
$\{[Cd(tipa)_2 \cdot (ClO_4)_2\}_n$	2D	41.9%		
$\{[Cd(tipa)(NO_3)_2\}_n$	1D	33.2%		
$\{[Cd_2(SO_4)_2(tipa)_2\}_n$	2D	28.3%		[54]
$\{[Cd(tipa)(NO_3)(SA)] \cdot (DMF)\}_n$	2D	none	sulfanilic acid	
$\{[Cd(tipa)(HCOO)_2 \cdot xG\}_n$	3D	25.3%		
$\{[Zn(TIPA)pim_0.5]2H_2O \cdot NO_3\}_n$	3D	26.6%	$H_2pim = pimelic\ acid$	[55]
$\{[Zn(TIPA)(pim)_3H_2O\}_n$	2D	38.4%		
$\{[WOS_3Cu_3Br(TIPA)] \cdot (H_2O)(DMF)\}_n$	3D	29.8%		[56]
$[Zn_4(Tipa)_4Cl_4] \cdot 4(G1)$	3D	none		
$[Zn_4(Tipa)_4Cl_4] \cdot 4(G2)$	3D	none		
$[Zn_2(Tipa)_2Cl_2] \cdot (G3)$	3D	none		
$[Zn_2(Tipa)_2(OH)] \cdot (G4)$	3D	none		[57]
$[Zn_3(Tipa)_2(OH)_3] \cdot (G5)$	3D	none		
$[Zn_3(Tipa)_2F_2(H_2O)_4] \cdot 2(G6)$	3D	none		
$[Cd(TIPA)(suc)_0.5(NO_3)_1H_2O]_n$	3D	none	succinic acid	[59]
$[Ni(TIPA)(tda)_{0.5}(H_2O)_1H_2O]_n$	3D	none	2,5-thiophenedicarboxylic acid	
$[Cd(TIPA)(tda)_{0.5} \cdot \frac{1}{2}H_2O]$	3D	none		
$\{[Zn(TIPA)(seb)_0.5](NO_3)_3 \cdot 3.5H_2O\}_n$	3D	none	$seb = sebacic\ acid$	
$[Zn_2(Tipa)(4,4')-$	3D	none		
$bpdcl_{1.5}(H_2O)(NO_3)_2 \cdot 2(DMF) \cdot H_2O$	3D	33.0%		[60]
$[Cd(Tipa)Cl_2] \cdot 2(DMF) \cdot H_2O$	3D	none		
$[Co(Tipa)Cl_2(H_2O)] \cdot DMF \cdot H_2O$	2D			
$[Zn_2(Tipa)_2(OH)] \cdot 3NO_3 \cdot 12H_2O$	2D	41.6%		
$[Zn_2(Tipa)_2(OH)] \cdot NO_3 \cdot Cr_2O_7 \cdot 5H_2O$	3D	none		[61]
$[Zn(Tipa)] \cdot 2NO_3 \cdot DMF \cdot 4H_2O$	3D	41.8%		
$[Zn_2(TIPA)_2(OH)(NO_3)_3] \cdot 5H_2O$	3D	49.0%		[62]
$[Zn_2(TIPA)_2(OH)(Cr_2O_7)_{1.5}] \cdot 3H_2O$	3D	none		
$[Ni(TIPA)(COO^-)_2(H_2O)] \cdot 2(DMF)_2$	2D	39.1%		[63]
$[Cd(TIPA)_2(ClO_4^-)_2] \cdot (DMF)_3(H_2O)$	2D	50.5%		
$\{[Ni_2(TIPA)_3(SO_4)(H_2O)_3] \cdot (SO_4) \cdot x(G)\}_n$	3D	24.6%		[64]
$[Zn_2(HPO_3)_2(TIPA)] \cdot 2H_2O$	2D	none		[65]
$[Zn_3(HPO_3)_3(TIPA)] \cdot 6H_2O$	1D	none		
$[Zn_3(Tipa)_2(Im)_3] \cdot 3NO_3 \cdot \text{solvent}$	3D	28.8%	$Im = imidazole$	
$[Zn_2(Tipa)_2(Tz)][Zn(Tipa)(NO_3)(H_2O)] \cdot 4NO_3 \cdot 3DOA$	2D	32.6%	$Tz = tetrazole, DOA = 1,4-dioxane$	[66]
$[Cd(tipa)(\mu_3-OH) \cdot NO_3 \cdot EtOH \cdot DMF]_n$	3D	none		[67]
$(Me_2NH_2)_3[(Ti_4L_6)Zn_3(OH)(tipa)_2] \cdot \text{Guests}$	3D	36.2%	$L = embonate$	[68]
$\{[Ni_2(L)_3(SO_4) \cdot (H_2O)_3] \cdot (HAsO_4) \cdot xG\}_n$	3D	none		[69]
$[Ni(tipa)_2](NO_3)_2$	2D	none		[70]
$[Zn_2(tipa)_2(OH^-)](NO_3^-)(SG7)_{2/3} \cdot 5H_2O$	3D	none	$SG7 = \text{solvent green 7}$	[71]
$\{[Zn(tipa)Cl] \cdot NO_3 \cdot 2DMF\}_n$	3D	37.4%		
$\{[Cd_2(tipa)_2Cl_4] \cdot 6DMF\}_n$	3D	none		
$\{[Zn_2(tipa)_2Cl_2] \cdot 2I_3 \cdot 2DMF\}_n$	3D	none		
$\{[Cd_2(tipa)_2Cl_2(dmf)_2] \cdot 2I_3 \cdot 4DMF\}_n$	3D	none		[72]

2.1. Small Organic Molecule as Auxiliary

The first TIPA-based cationic MOF with nanoscaled channels was prepared by our group [61]. When we prepared a MOF consisting of TIPA and int (isonicotinic acid), we tried to synthesize a new MOF by replacing int with L-proline, because L-proline is a chiral molecule and has a similar size to int. As a result, a new framework, namely FIR-53 (FIR = Fujian Institute Research), was synthesized. FIR-53 has a double layer structure. The μ_3 -TIPA ligands connect Zn^{2+} ions to yield a single layer, which is then bridged over each other to form a dual-sheet structure by Zn-OH-Zn units. The overall framework is a non-interpenetrated network with 41.6% porosity that has one-dimensional ellipse channels along the c axis, with a window size of approximately $18 \times 13 \text{ \AA}^2$ (Figure 2a). Importantly, this framework has extremely high stability in water and air, and we can obtain an accurate structure using Single-Crystal X-ray diffraction after being exposed in water and air one year.^{897/*}

Inspired by this, other amino acids have been used as regulators. FIR-54 was also prepared with L-proline as the regulator. FIR-54 is a 2-fold interpenetrating cationic framework, featuring one-dimensional large channels with a cross section of $10.5 \times 10.5 \text{ \AA}^2$ (Figure 2b). Generally, these kinds of organic molecules do not appear in the final compositions of coordination compounds; perhaps they played the roles of structure direct agents (SDAs), similar to organic amines in the formation of zeolites. Another cationic framework $[Zn_2(TIPA)_2(OH)(NO_3)_3] \cdot 5H_2O$ [62] is the supramolecular isomer FIR-53. The framework contains four kinds of channels, the smallest apertures are 5.6, 5.4, 4.0, and 2.4 \AA , respectively (Figure 2c). Through the assistant of glycine, $[Ni(TIPA)(COO^-)_2$

$(\text{H}_2\text{O}) \cdot 2 (\text{DMF})_2 (\text{H}_2\text{O})$ [63] was synthesized. The framework has a one-dimensional nano-scaled channel along the c-axis with a window size of $6.3 \times 7.2 \text{ \AA}^2$. All of these frameworks exhibited a high porosity and high stability in water, common organic solvent, and air.

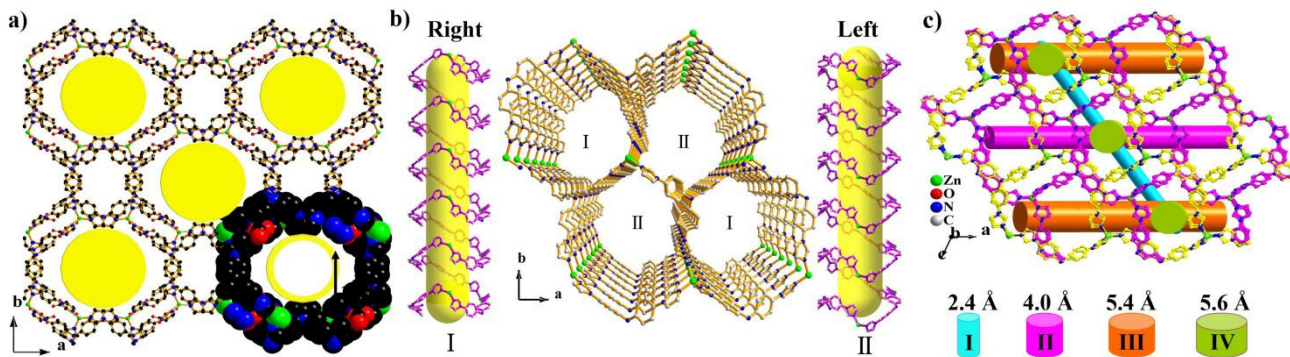


Figure 2. (a) Open framework with large channels in FIR-53. (b) Open framework with large channels in FIR-54. (c) Open framework with large channels in $[\text{Zn}_2 (\text{TIPA})_2 (\text{OH}) (\text{NO}_3)_3] \cdot 5\text{H}_2\text{O}$. Reproduced with permission [58]. Copyright 2020, the American Chemical Society.

2.2. Inorganic Oxyanion as Auxiliary

Another strategy to prepare TIPA-based porous frameworks is to adopt inorganic oxyanions as auxiliaries; the inorganic oxyanions can bridge metal center ions to yield metal-oxyanion subunits. SO_4^{2-} , PO_4^{3-} and HPO_3^{2-} are always selected preferentially as they are known to bind strongly with metal nodes. A water-stable cationic MOF $\{[\text{Ni}_2 (\text{L})_3 (\text{SO}_4)^- (\text{H}_2\text{O})_3]\cdot(\text{SO}_4)\cdot x\text{G}\}_n$ ($1'\text{-SO}_4$; L = tris (4-(1H-imidazol-1-yl)phenyl) amine; G = DMF, H_2O) with a 3D framework was reported by Ghosh [64]. The asymmetric unit contains two sulphate anions, one is connected to the Ni^{2+} ions, while the other is a free counterion in the space. The total free volume of the compound is 4592.83 \AA^3 , which corresponds to 24.6% of the total volume. This framework has high hydrolytic stability. Two hybrid zincophosphites $[\text{Zn}_2 (\text{HPO}_3)_2 (\text{TIPA})] \cdot 2\text{H}_2\text{O}$ and $[\text{Zn}_3 (\text{HPO}_3)_3 (\text{TIPA})] \cdot 6\text{H}_2\text{O}$ [65] were prepared through the assembly of TIPA and phosphite, both of which feature inorganic zincophosphate chains as supramolecular building blocks.

2.3. Small Organic Molecule as Secondary Linker

In theory, it is reliable to use longer linkers to synthesize MOFs with larger pores; however, there are dozens of examples where MOFs were prepared using TIPA and carboxylates as colinkers, and almost no highly porous MOFs were constructed. Considering that the highly porous framework, FIR-53, was assembled through the stacking of $[\text{Zn}_2 (\text{TIPA}) (\text{OH})]^{3-}$ layers, small molecule imidazole and imidazole and its derivatives can also adopt a μ_2 -coordination mode which is similar to -OH. On the basis of this strategy, two MOFs, namely, $[\text{Zn}_3 (\text{TIPA})_2 (\text{Im})_3] \cdot 3\text{NO}_3 \cdot \text{solvent}$ (Im = imidazole) with a three-dimensional (3D) pillared-layer framework and $[\text{Zn}_2 (\text{TIPA})_2 (\text{Tz})][\text{Zn}(\text{TIPA})(\text{NO}_3)(\text{H}_2\text{O})] \cdot 4\text{NO}_3 \cdot 3\text{DOA} \cdot \text{solvent}$ (Tz = tetrazole, DOA = 1,4-dioxane) [66] with a rare sandwich structure were synthesized. The former compound has a kind of large elliptic channel, with pore apertures of 7.7 and 13.1 \AA along the a axis, and the free NO_3^- ions are located inside the channels. In the structure view of the latter compound, each Zn^{2+} ion adopts the four-connected model, linked by three TIPA molecules to generate a single layer, further bridged by μ_2 -Zn-Tz-Zn units to form a bilayer structure with an open window of ca. 11.0 \AA (Figure 2c). These two compounds have a porosity of 32.6% and 28.8%, respectively.

2.4. Metal Clusters as Nodes

Using polynuclear clusters, especially, high-nuclear clusters, such as hexa-, octa-, dode-nuclear and greater, as building units has been demonstrated as a feasible strategy to

construct highly porous MOFs [73–76]. To some extent, polynuclear clusters can endow highly-connected numbers and further decrease steric hindrance of organic ligands around them. Rationally selecting the origin of clusters and modulators of synthesis processes could promote the synthesis of targeted structures.

Sun's group reported an unprecedented (3,12)-connected MOF, $[\text{Cd}(\text{TIPA})(\mu_3\text{-OH})\cdot\text{NO}_3\cdot\text{EtOH}\cdot\text{DMF}]_n$ [67] with a ttt topology based on cubic $[\text{Cd}_4(\mu_3\text{-OH})_4]$ clusters and TIPA ligands (Figure 3d,e). Each Cd^{2+} ion adopted an octahedral configuration coordinated by three nitrogen atoms from three independent TIPA molecules and three oxygen atoms from three independent $\mu_3\text{-OH}^-$. Four crystallographically equivalent $\text{Cd}(\text{II})$ ions are bridged by four $\mu_3\text{-OH}^-$ ions to yield cubic and 12-connected $[\text{Cd}_4(\mu_3\text{-OH})_4]$ clusters where Cd and O alternatively located at the corners. The μ_3 -coordinated TIPA ligands connected with $[\text{Cd}_4(\mu_3\text{-OH})_4]$ clusters to form a three-dimensional framework with moderate pores. A stepwise assembly strategy was established for the construction of Ti-MOFs by our group. Particularly, the combination of Ti_4L_6 (L = embonate) cages, metal ions and our ligands provide an efficient approach to prepare Ti_4L_6 -cage-based MOFs. By selecting TIPA as auxiliary ligands, a network of PTC-220 ($\text{Me}_2\text{NH}_2)_3$ $[(\text{Ti}_4\text{L}_6)\text{Zn}_3(\text{OH})(\text{TIPA})_2]\cdot$ guests [68] was constructed (Figure 3a–c). In PTC-220, the ligand adopts a μ_3 -coordinated mode to connect Zn^{2+} ions into an one-dimensional chain, Ti_4L_6 cages are bridged Zn^{2+} ions that form a ladder-shaped chain. These two kinds of chains are mutually crosswise arranged to result in a three-dimensional framework, and this framework consists of two types of channels with relative dimensions of $7 \times 14 \text{ \AA}^2$ and $6 \times 6 \text{ \AA}^2$, respectively (Figure 3d). Our group also prepared a porous framework $[\text{Cd}(\text{TIPA})\text{Cl}_2\cdot 2(\text{DMF})\cdot\text{H}_2\text{O}]_n$ [60] based on a 6-connected Cd_2Cl_4 cluster. The assembly of $\text{Cd}(\text{II})$ ions and TIPA molecules generated a three-dimensional framework with large channels. The isolated frameworks are further joined by $\mu_2\text{-Cl}^-$ ions to form a double-walled network. The final 2-fold interpenetrating structure has a solvent-accessible void space of 33.0% of the total crystal volume.

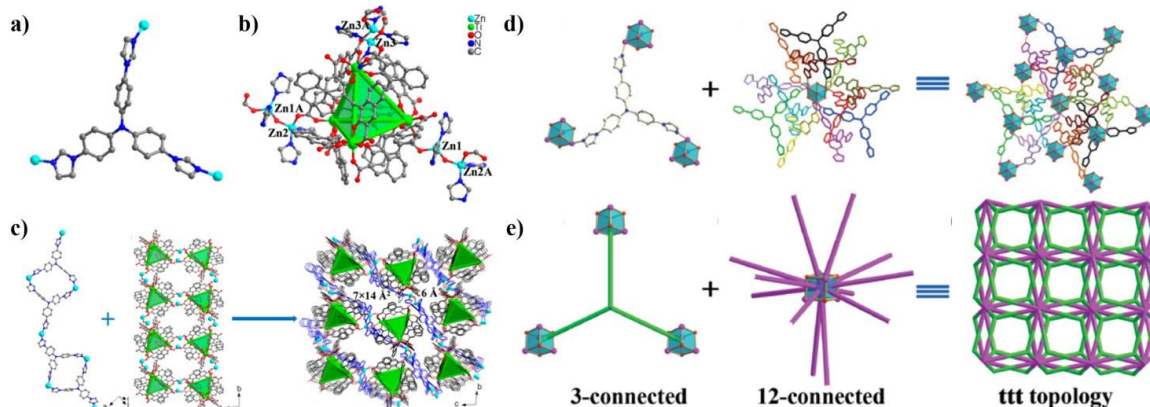


Figure 3. (a) Coordination environment of TIPA ligand. (b) Coordination model of the Zn^{2+} atoms, and Ti_4L_6 cage in PTC-220. (c) Zn atoms linking the TIPA ligands into a chain, and Zn atoms linking the Ti_4L_6 cages into a ladder-shaped chain, 3D framework of PTC-220 with different pore sizes. Reproduced with permission [75]. Copyright 2020, the American Chemical Society. (d) A 3-connected TIPA ligand and simplified 3-connected linker. (e) A 12-connected $[\text{Cd}_4(\mu_3\text{-OH})_4]$ cubic cluster and simplified 12-connected node, (3,12)-connected framework and the ttt topology. H atoms removed for clarity. Reproduced with permission [67]. Copyright 2014, Royal Society of Chemistry.

3. The Application of TIPA-Dominated Porous MOFs

3.1. The Capture of Toxic Oxoanions

Several cationic frameworks with high porosity and high stability were prepared using TIPA as linkers. Reported by our group, two cationic MOFs (FIR-53 and FIR-54) [58] with nanoscale channels exhibited that high capacity of chromium exceeding 100 mg g^{-1} compounds also displays fast and efficient trapping-releasing processes. Importantly, the single crystal of the chromium-loaded sample was also subject to Single-Crystal X-ray

diffraction. It was found that $\text{Cr}_2\text{O}_7^{2-}$ ions existed in the double layer instead of NO_3^- anions. In addition, another cationic framework $[\text{Zn}_2(\text{TIPA})_2(\text{OH})(\text{NO}_3)_3] \cdot 5\text{H}_2\text{O}$ [62] with the same formula as FIR-53, also acted as a single crystal container to trap Cr (VI)-oxyanions in a SC-SC fashion (Figure 4c,d). It exhibited a fast sorption kinetics toward Cr (VI)-oxyanions in water with high selectivity, as well as good repeatability. Interestingly, CrO_4^{2-} rather than $\text{Cr}_2\text{O}_7^{2-}$ was confirmed in the channel from the single crystal structure. This was mainly ascribed to the spatial confinement of the channels. It was revealed that the electrostatic interaction and rich hydrogen bonds between the CrO_4^{2-} ions and the framework played an important role in the capture of CrO_4^{2-} ions. In addition, FIR-54 also has the high-performance adsorption behaviors of Cr (VI)-oxyanions in aqueous solutions, although the crystals remains intact after ion exchange, the existence of counterions could not be found from the Cr (VI)-oxyanion-exchanged samples, and only the accurate structure of host framework was obtained by Single-Crystal diffraction. Compared the sorption results of these three compounds, it could be determined that the size effect of the pores played a crucial role in the existence of the formation of Cr (VI)-oxyanions, largely affecting the aggregate state. These results are remarkably important to prepare practical materials for Cr (VI)-oxyanion capture.

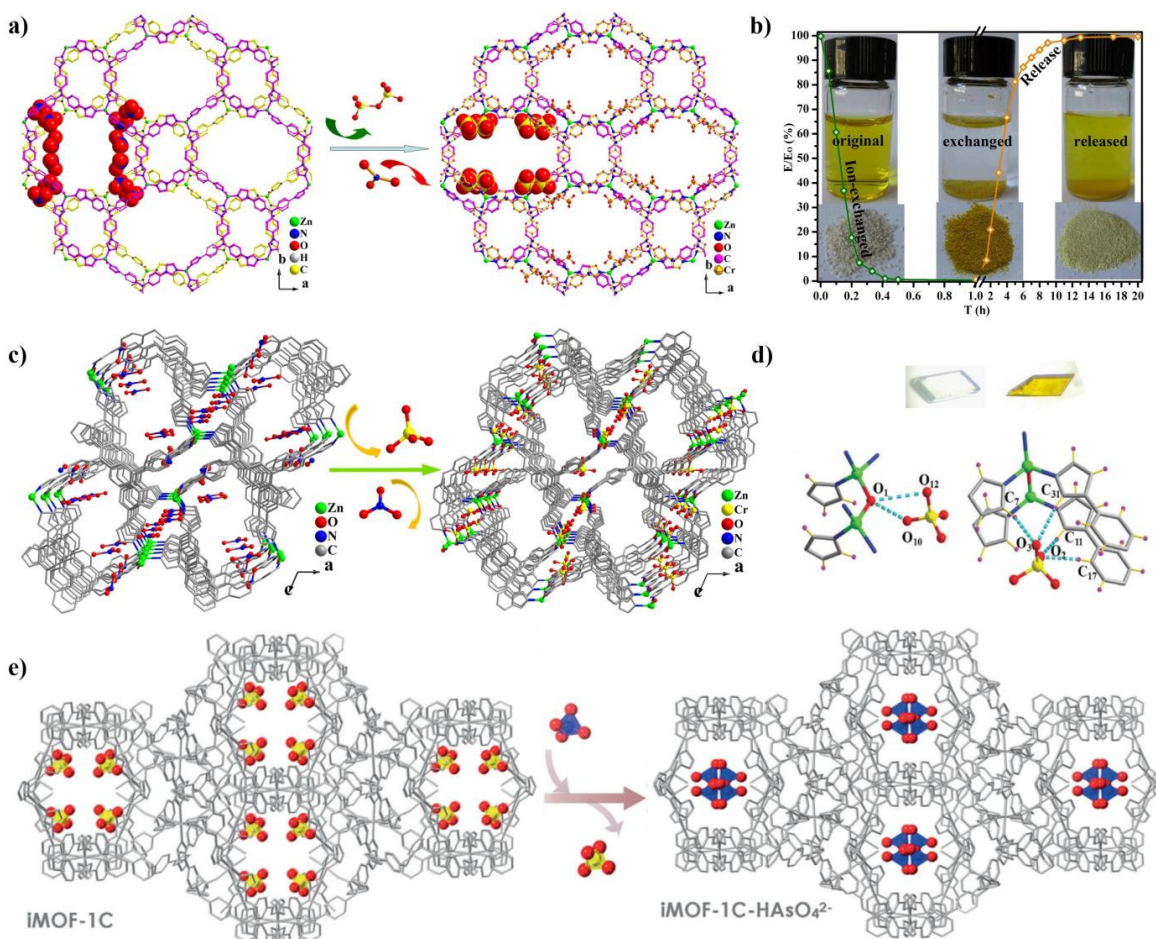


Figure 4. (a) Structures of FIR-53 before and after ion exchange: 3D structure of FIR-53 containing NO_3^- along the c axis, 3D structure of FIR-53 containing $\text{Cr}_2\text{O}_7^{2-}$ along the c axis. (b) Photographs show the color of crystals before and after trapping–releasing process. Reproduced with permission [58]. Copyright 2015, the American Chemical Society. (c) A 3D structure of compound $[\text{Zn}_2(\text{TIPA})_2(\text{OH})(\text{NO}_3)_3] \cdot 5\text{H}_2\text{O}$ along the b-axis: NO_3^- ions as guests in the channels, CrO_4^{2-} ions instead of NO_3^- located in the channels. (d) H bonds between the framework and CrO_4^{2-} , color change of FIR-53 crystals before and after ion exchange. Reproduced with permission [62]. Copyright 2018, Royal Society of Chemistry. (e) Packing diagram representing Single-Crystal-to-Single-Crystal transformation of parent cationic MOF, iMOF-1C, to HAsO_4^{2-} encapsulated phase. Reproduced with permission [67]. Copyright 2020. John Wiley & Sons, Ltd.

Ghosh et al. reported a water-stable cationic MOF $\{[\text{Ni}_2(\text{L})_3(\text{SO}_4)_2(\text{H}_2\text{O})_3]\cdot(\text{SO}_4)\cdot\text{xG}\}_n$ ($\text{L}'=\text{SO}_4$; $\text{L}=\text{tris (4-(1H-imidazol-1-yl)phenyl) amine}$; also referred to as iMOF-1C, G = guest solvent molecules and C = Cationic) (Figure 4e) [69]. MOF 1-SO₄ can act as dual adsorbent for permanganate ions and dichromate. This compound exhibits a moderate capacity of about 166 mg g⁻¹ for Cr₂O₇²⁻ ions. Although both the crystallinity and integrity of the framework after the exchange was retained, the crystal structure of 1-SO₄ after saturated adsorption by SC-XRD was unsuccessful due to the poor diffraction. Meanwhile, this group used iMOF-1C as an efficient ion-exchanger to capture the toxic oxoanions selenium (SeO₄²⁻) and arsenic (HAsO₄²⁻) from an aqueous medium. Interestingly, it exhibited fast kinetics and high sorption capacity, 100 mg g⁻¹ and 84 mg g⁻¹ for SeO₄²⁻ and HAsO₄²⁻, respectively, which are among the highest values reported in the field of MOFs. A Single-Crystal structure, after arsenate and selenate oxoanion, could be obtained, monohydrogen arsenate and selenate anion replace the sulfate anion along the 1D channel of the framework. This result could be attributed to the effect of the charge and geometry, where the SeO₄²⁻ and HAsO₄²⁻ anions are tetrahedral and have similar shapes and sizes to SO₄²⁻. The adsorption of iMOF-1C provided a typical example to reveal the exchange mechanism for the removal of hazardous toxic oxoanions. Our group reported a two-dimensional cationic framework, namely [Cd (TIPA)₂] (ClO₄⁻)₂·(DMF)3 (H₂O) [62]; it was employed an ion-exchange material for the capture of Cr₂O₇²⁻ anions. The capture capacity of this compound was up to 116.6 mg g⁻¹. This compound also showed excellent selectivity, and the adsorption ability of Cr (VI) was not significantly affected, in addition, the concentration of various types of anion species was five times higher than that of the Cr₂O₇²⁻ anion. Importantly, it has the excellent reusability. The guest-loaded MOFs were immersed in KNO₃ aqueous solution, up to 92% Cr₂O₇²⁻ anions were released again into the solutions after 24 h. This compound maintained approximately 81% release efficiency during five continuous cycles. In the work of Wang's group, an isomorphic structure was reported using Ni²⁺ ions as nodes [70]. It exhibited high alkaline stability and exceptional ⁹⁹TcO₄⁻ capture selectivity. Liquid scintillation counting (LSC) measurements verified that this compound exhibited extremely rapid kinetics with an equilibrium time of ~5 min; this can be largely attributed to the nature of the layered structure, which is in favor of the diffusion and transportation of anions. Moreover, the high positive charge density and hydrophobicity also increased the affinity of the 2D layers for ⁹⁹TcO₄⁻ anions. In addition, similar exchange kinetics were found for ReO₄⁻ anions. The maximum anion-exchange capacity of the ReO₄⁻ anions was 318 ± 8 mg/g. Of significance, this compound exhibited fairly high adsorption amounts of ReO₄⁻ removal, even SO₄²⁻ was present in a 6000-fold excess. These results make it an extremely viable candidate for the selective removal of ReO₄⁻/⁹⁹TcO₄⁻ from waste solutions.

3.2. Sensing

MOFs as a class of luminescent materials largely depend on ligands and metal nodes. The powder of TIPA itself has weak blue emission; however, the emission intensity is greatly enhanced via crystallization, where the orientation and arrangement of TIPA molecules was improved and the rigidity was increased. In Fu's contribution, [Cd (TIPA)₂] (ClO₄⁻)₂·(DMF)3 (H₂O) was used as a luminescent probe to detect anions in aqueous media 62. This compound exhibited high selectively against Cr₂O₇²⁻ anions among (BF₄⁻, VO₄³⁻, MoO₄²⁻, WO₄²⁻, ClO₄⁻, SO₄²⁻, NO₃⁻, Br⁻, Cl⁻, I⁻, SCN⁻, OAc⁻ and OX₂⁻). The K_{sv} value was calculated to be 7.15×10^4 L mol⁻¹ and the detection limit was as low as 8 ppb (S/N = 3), which matched that of the reported MOFs. Guo et al. prepared self-interpenetrating MOFs [CdL (NO₃⁻)₂·4H₂O]_n ($\text{L}=\text{tris (4-(1H-imidazol-1-yl)phenyl) amine}$) [77], which has a high water stability. This compound was implemented as luminescent sensors to monitor antibiotics in aqueous solutions. This MOF has excellent selectivity towards NFT and a K_{sv} value of NFT as high as 4.64×10^4 M⁻¹.

Beyond this, the inherent porous nature of MOFs enables the encapsulation of versatile chromophore guests into the MOF pores to construct multiple-luminescence MOFs. For

example, our group selected SG7 (solvent green 7, a sulfonated pyrene) as a guest with green emissions as the precursors of FIR-53 to prepare SG7@FIR-53 via an ion-exchange route [71]. SG7 is a normal dye molecule for fluorescence chemistry. The parent MOF exhibited ultrahigh stability and the crystallinity and morphology maintained excellent integrity in water or air for at least six months during the ion-exchange period. The color of the crystals gradually became transparent to yellow green. SG7@FIR-53 showed dual emission at 375–455 and 500–550 nm under the single excitation wavelength at 310 nm, while the free TIPA ligand and FIR-53 displayed similar blue emissions in the range from 375 to 470 nm, indicating that SG7 was introduced inside the channels and existed in the form of excimer aggregation; by comparison, the monomer emission of SG7 (pyrene) was during 375–405 nm [78]. In order to verify this hypothesis of excimer aggregation, we attempted to obtain the crystal structure of the guest-loaded framework. We determined up the dye-exchanged MOF when the ion-exchange process lasted a month. Fortunately, the structure of the SG7-encapsulated FIR-53 was successfully obtained via the Single-Crystal X-ray diffraction method. SG7³⁻ instead of NO₃⁻ anions located on the sides of the channels further formed a paralleled double layer in the direction of the c axis; the distance of the adjacent SG7³⁻ ions was approximately 10 Å (Figure 5a,b). The stacking of the SG7³⁻ anions indicated that it yielded the excimer emission of pyrene, which is coincident with the fluorescence spectra analysis. To the best of our knowledge, it is the first report where the introduction of dye into MOF was achieved via SC-SC transformation. Different anions were detected in aqueous solution though the fluorescence changes of SG7@FIR-53; it was found that Cr₂O₇²⁻ or MnO₄⁻ showed a marked quenching effect on SG7@FIR-53 and the detection limit was calculated as low as 1.02 and 0.12 ppb, respectively.

We also introduced 8-hydroxy-1,3,6-pyrenetrisulfonicacid trisodium salt (HPTS) into a cationic MOF [Zn (TIPA) (NO₃⁻) (H₂O)]·5H₂O, which has the same framework as FIR-54. HPTS powder has no fluorescence owing to the Aggregation-Caused Quenching effect; however, MOF·HPTS show the bright green emission [79]. By fluorescence measurement, the complex MOF·HPTS shows a dual-emitting behavior at around 375–450 and 500–575 nm, belonging to the blue emission of TIPA and the green emission of HPTS, respectively (Figure 5c–e). It is worth mentioning that MOF·HPTS showed an intensive emission with only a slight reduction after 60 days in air and aqueous solution, respectively. This result indicated that the confinement effect of the porous network could protect the aggregation state of fluorescent dyes and effectively suppress Aggregation-Caused Quenching. MOF·HPTS can serve as a durable dual-emitting sensor. MOF·HPTS exhibited the obvious quenching effects towards a wide range of aromatic nitro-explosives in aqueous solution. If fluorescence emission of HPTS is the reference, the concentrations of TNP, 2-NP, 3-NP, and 4-NP caused the complete quenching of MOF·HPTS as low as 50 ppm. Importantly, MOF·HPTS showed high sensitivity to aliphatic nitro-compounds. DMNB (2,3-dimethyl-2,3-dinitrobutane) and RDX (1,3,5-triazine) and HMX (cyclotetramethylenetrinitramine) caused almost total quenching of HPTS at a low concentration below 100 ppm. Especially, MOF·HPTS exhibited a ratiometric fluorescence sensing for RDX detection, with increasing concentration of RDX, the emission intensity of HPTS decreased sharply, while the blue emission at 400 nm was greatly strengthened (Figure 5f). So far, it is the only example among luminescent sensors that has the ratiometric fluorescence effect against RDX. In addition, MOF·HPTS exhibits a high response to a broad class of nitro-containing antibiotics.

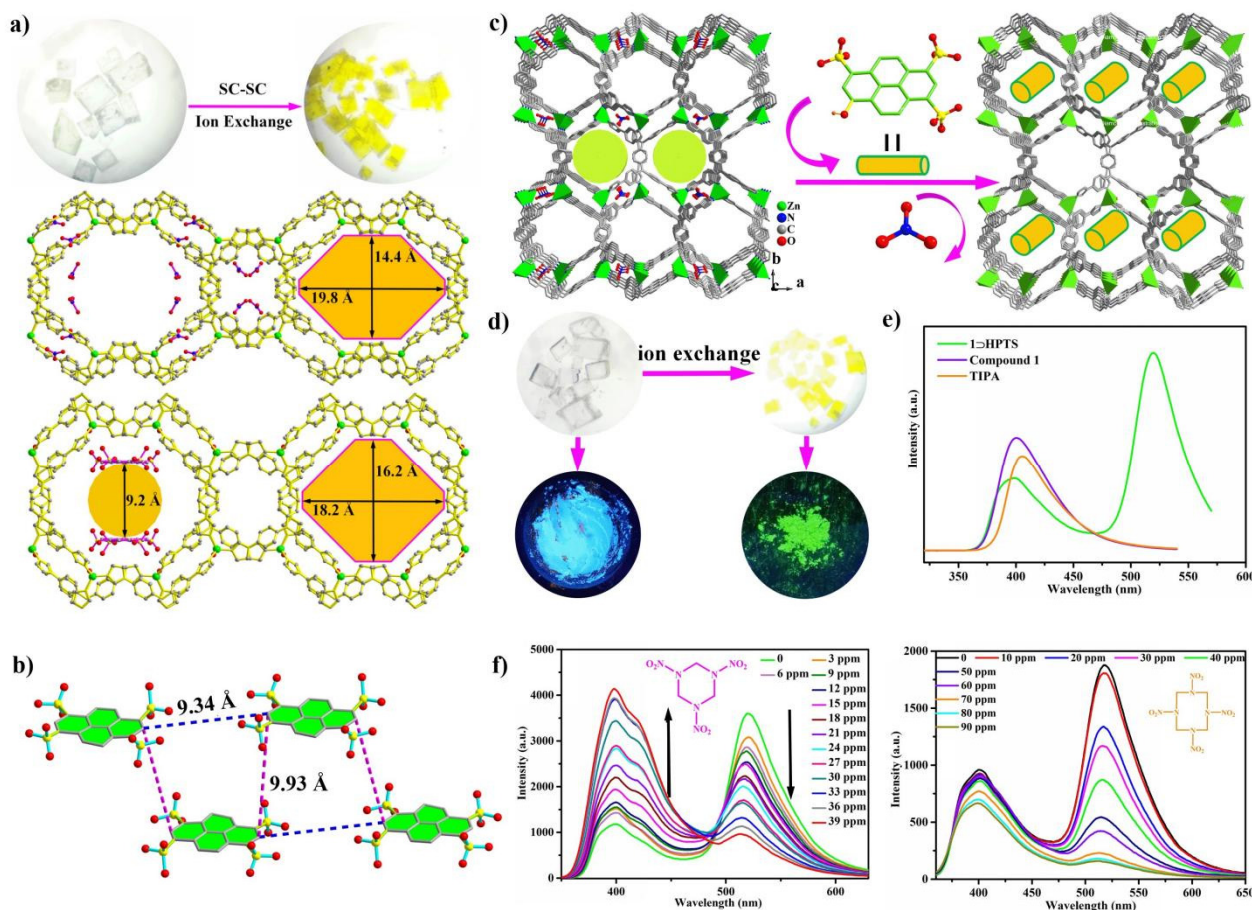


Figure 5. (a) Photograph of FIR-53 crystals, 3D framework of FIR-53 along the c axis, the window size from $19.8 \times 14.4 \text{ \AA}^2$ of FIR-53 to $20.2 \times 17.3 \text{ \AA}^2$ of SG7@FIR-53 along c axis. (b) Photograph of FIR-53 after ion exchange, the arrangement and configuration of SG73– along the two sides of the channels. Reproduced with permission [69]. Copyright 2018, the American Chemical Society. (c) A 3D framework of compound FIR-54 after ion exchange. (d) Photographs show the colors of crystals before and after the trapping process in the two images above, and the fluorescence emission of the crystal powder before and after ion exchange under ultra-violet light in the two images below. (e) Photographs show the solid-state fluorescence emission of compound FIR-54, TIPA, and MOFÉHPTS. (f) The fluorescence titrations of MOFÉHPTS upon exposure to the aqueous solution of RDX and HMX. Reproduced with permission [79]. Copyright 2018, Royal Society of Chemistry.

3.3. Gas Adsorption

The high stability and the rich porous environment of these TIPA-based frameworks enabled these MOFs to serve as excellent adsorbents for the storage and purification of gas molecules. Our group reported a nonporous MOF with gas adsorption selectivity, $[\text{Cd}(\text{TIPA})\text{Cl}_2] \cdot 2(\text{DMF}) \cdot \text{H}_2\text{O}$ [60], which has a two-fold interpenetrated framework composed of a dinuclear Cd_2Cl_2 unit and TIPA. This compound displays the typical type I sorption of N_2 with a BET surface area of $348.8 \text{ m}^2 \text{ g}^{-1}$. This compound has a moderate adsorption capacity of C_2H_2 ($64.13 \text{ cm}^3 \text{ g}^{-1}$) and C_2H_4 ($40.52 \text{ cm}^3 \text{ g}^{-1}$) and CH_4 ($12.04 \text{ cm}^3 \text{ g}^{-1}$) at 297 K and 1 atm (Figure 6a,b); however, the Q_{st} (adsorption isosteric heat) values of C_2H_2 and C_2H_4 were 41.05 and 34.69 kJ/mol, respectively, indicating strong solid-gas interactions between the framework and the small gas molecules. As a result, the adsorption selectivity of $\text{C}_2\text{H}_2/\text{CH}_4$ and $\text{C}_2\text{H}_4/\text{CH}_4$ was 39.1 and 13.5 at 297 K, respectively. A 2D + 2D \rightarrow 3D interpenetrating framework $[\text{Ni}(\text{TIPA})(\text{COO}-)_2(\text{H}_2\text{O})] \cdot 2(\text{DMF}) \cdot 2(\text{H}_2\text{O})$ [63] was prepared for small hydrocarbon separations. The surface area was $404.6 \text{ m}^2 \text{ g}^{-1}$ measured by the CO_2 adsorption at 195 K. This porous material exhibited moderate capacity of C_2H_2 and CO_2 , 65.8 and $46.9 \text{ cm}^3 \text{ g}^{-1}$ at 273 K, 56.8 and $39.0 \text{ cm}^3 \text{ g}^{-1}$ at room temperature (Figure 6c,d). The adsorption selectivity of $\text{C}_2\text{H}_2/\text{CH}_4$ and $\text{C}_2\text{H}_2/\text{CO}_2$ (equimolar binary mixtures) was

calculated using the ideal adsorption solution theory (IAST) at 273 and 297 K, the selectivity of $\text{C}_2\text{H}_2/\text{CH}_4$ and $\text{C}_2\text{H}_2/\text{CO}_2$ in this compound is 112.2 and 8.0 at 297 K, and 228.6 and 6.1 at 273 K. The $\text{C}_2\text{H}_2/\text{CH}_4$ selectivity is the highest one among MOFs-based materials to date [80] and was largely attributed to the confined ultra-microporous channel (the channel size was $6.3 \times 7.2 \text{ \AA}^2$) and the naked carboxylic group, which enhanced the interactions with C_2H_2 molecules.

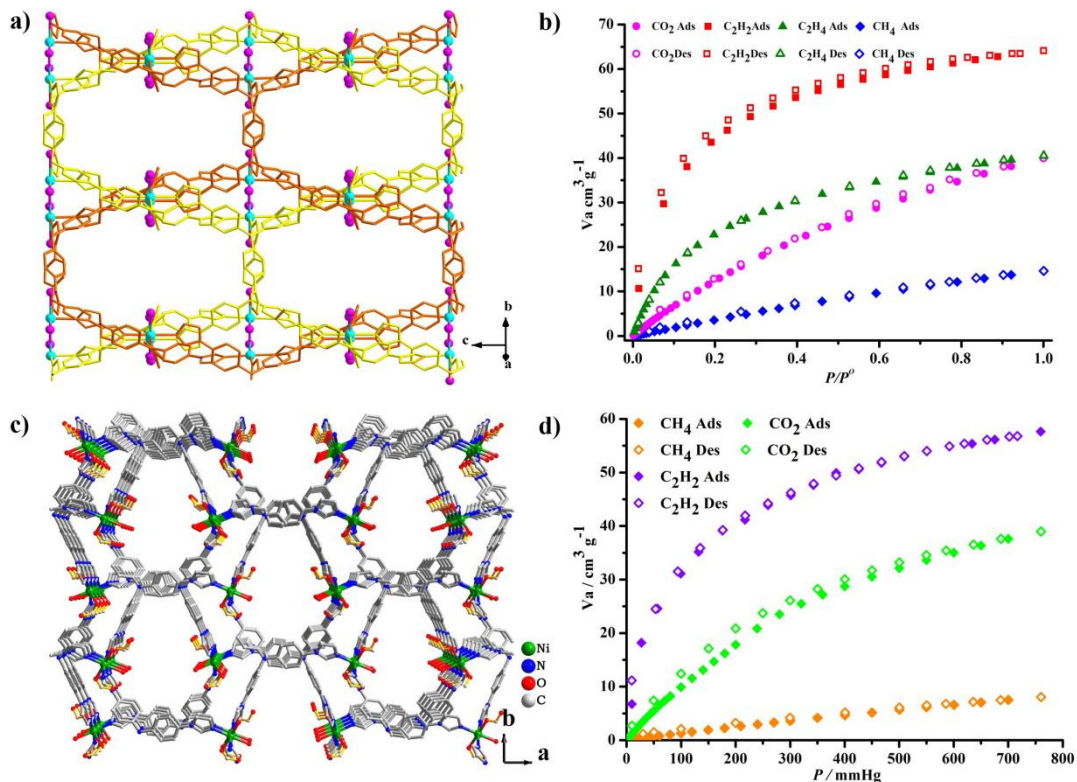


Figure 6. (a) A simple framework containing two Cd-TIPA frameworks linked by $\mu_2\text{-Cl}^-$ ions. (b) C_2H_2 , C_2H_4 , CH_4 and CO_2 sorption isotherms at 297 K. Reproduced with permission [60]. Copyright 2014, the American Chemical Society. (c) 3D framework of compound $[\text{Ni}(\text{TIPA})(\text{COO}^-)_2(\text{H}_2\text{O})] \cdot 2(\text{DMF})_2(\text{H}_2\text{O})$ along the c axis. (d) adsorption isotherms of CO_2 , CH_4 and C_2H_2 at 297 K. Reproduced with permission [63]. Copyright 2018, Royal Society of Chemistry.

4. Conclusions

In this article, different methods to prepare highly porous MOFs with high stability using neutral nitrogen-based ligand TIPA, without carboxyl ligands, was briefly introduced. These porous crystalline materials have been successfully applied in the adsorption of toxic oxoanions, luminescent sensing, including cations, anions, aromatic explosives, and aliphatic nitro-compounds, and the storage and purification of small molecule gases.

TIPA as linkers, exhibits huge advantages in constructing porous MOFs; they can, not only be used to build highly stable and porous frameworks to capture several kinds of toxic oxoanions (CrO_4^{2-} , $\text{Cr}_2\text{O}_7^{2-}$, SeO_4^{2-} and HAsO_4^{2-}) in aqueous media via the SC-SC approach, but they can also be used to synthesize porous host frameworks to encapsulate guest emitters to create multiple emitting systems [81–83].

Although TIPA-based MOFs materials have made great achievements in synthesis and in various applications, some challenges remain to be critically solved. For example, more novel strategies were exploited to enlarge the scope of MOFs with high stability and porosity. Perhaps it is an efficient method to construct highly porous MOFs through a combination of various Ag clusters. In addition, the triphenylamine core of the ligand is a typical octupolar nonlinear optical chromophore and is known for two photon absorption-upconverted emission [84]. It is possible that TIPA-based MOFs can supply a new platform

for the development and application of polarized light materials and upconversion materials. Through the preparation of chiral MOFs, new materials for circularly polarized luminescence can be provided. In recent years, phosphorescence has shown unique properties, such as a long lifetime, large stoke shift, and abundant excited states, and has been a hotspot in the optoelectronic filed [85]. TPA derivatives have been widely used to develop purely organic phosphorescence [86–89], and one TIPA-based MOF showing the phosphorescence property was reported in 2014 [72]; it is still the only one reported to this day. If phosphorescence is efficiently integrated into MOFs, more interesting and significant applications can be promoted. Despite the fact that several MOFs were selected as host platforms for the encapsulation or capture of some guests, this work focused primarily on toxic oxoanions and organic small molecules, those of other structures, such as carbon dots and perovskite dots, have not been explored. More efforts are consequently essential to prepare these kinds of host-guest materials, with the introduction of carbon dots and perovskite dots into rigid matrices, and will provide a lot of other new functions (e.g., room temperature phosphorescence, light-emitting diodes, and laser). We believe that, with further in-depth research and innovation, a bright future for TIPA-based porous MOFs can be expected.

Author Contributions: H.F. and Y.J. contributed equally to this work. Writing—original draft preparation, H.F. and Y.J.; supervision and funding acquisition, F.W. and J.Z. All authors have read and agreed to the published version of the manuscript.

Funding: This research was funded by the National Natural Science Foundation of China (No. 21971241, U1904183) and the Talent Program of Henan Province (No. 20HASTIT006, 212300410061).

Institutional Review Board Statement: Not applicable.

Informed Consent Statement: Not applicable.

Data Availability Statement: The data presented in this study are available in the cited references.

Conflicts of Interest: The authors declare no conflict of interest.

References

1. Eddaoudi, M.; Moler, D.B.; Li, H.L.; Chen, B.L.; Reineke, T.M.; O’Keeffe, M.; Yaghi, O.M. Modular Chemistry: Secondary Building Units as a Basis for the Design of Highly Porous and Robust Metal–Organic Carboxylate Frameworks. *Acc. Chem. Res.* **2001**, *34*, 319–330. [[CrossRef](#)]
2. Feng, L.; Wang, K.; Day, G.S.; Ryder, M.R.; Zhou, H. Destruction of Metal-Organic Frameworks: Positive and Negative Aspects of Stability and Lability. *Chem. Rev.* **2020**, *120*, 13087–13133. [[CrossRef](#)] [[PubMed](#)]
3. Zhao, Y.; Zeng, H.; Zhu, X.; Lu, W.; Li, D. Metal-Organic Frameworks as Photoluminescent Biosensing Platforms: Mechanisms and Applications. *Chem. Soc. Rev.* **2021**, *50*, 4484–4513. [[CrossRef](#)] [[PubMed](#)]
4. Liu, J.; Mukherjee, S.; Wang, F.; Fischer, R.A.; Zhang, J. Homochiral Metal-Organic Frameworks for Enantioseparation. *Chem. Soc. Rev.* **2021**, *50*, 5706–5745. [[CrossRef](#)] [[PubMed](#)]
5. Ding, M.; Flaig, R.W.; Jiang, H.; Yaghi, O.M. Carbon Capture and Conversion Using Metal-Organic Frameworks and Mof-based Materials. *Chem. Soc. Rev.* **2019**, *48*, 2783–2828. [[CrossRef](#)]
6. Zhang, X.; Wang, B.; Alsalmec, A.; Xiang, S.; Zhang, Z.; Chen, B. Design And Applications of Water-Stable Metal-Organic Frameworks: Status and Challenges. *Coord. Chem. Rev.* **2020**, *423*, 213507. [[CrossRef](#)]
7. Tian, D.; Liu, X.; Feng, R.; Xu, J.; Chen, R.; Huang, L.; Bu, X. Microporous Luminescent Metal-Organic Framework for a Sensitive and Selective Fluorescence Sensing of Toxic Mycotoxin in Moldy Sugarcane. *ACS Appl. Mater. Interfaces* **2018**, *10*, 5618–5625. [[CrossRef](#)]
8. Yao, Z.; Li, G.; Xu, J.; Hu, T.; Bu, X. A Water-Stable Luminescent ZnII Metal-Organic Framework as Chemosensor for High-Efficiency Detection of CrVI-Anions ($\text{Cr}_2\text{O}_7^{2-}$ and CrO_4^{2-}) in Aqueous Solution. *Chem. Eur. J.* **2018**, *24*, 3192–3198. [[CrossRef](#)]
9. He, J.; Xu, J.; Yin, J.; Li, N.; Bu, X. Recent Advances in Luminescent Metalorganic Frameworks for Chemical Sensors. *Sci. China Mater.* **2019**, *62*, 1655–1678. [[CrossRef](#)]
10. Wu, Y.P.; Tian, J.W.; Liu, S.; Li, B.; Zhao, J.; Ma, L.F.; Li, D.S.; Lan, Y.Q.; Bu, X. Microporous Metal-Organic Frameworks with Cubane $[\text{M}_4(\text{OH})_4]$ ($\text{M}=\text{Ni}, \text{Co}$) Clusters and Pore-Space Partition for Electrocatalytic Methanol Oxidation Reaction. *Angew. Chem. Int. Ed.* **2019**, *58*, 12185–12189. [[CrossRef](#)]
11. Fu, H.R.; Wang, N.; Wu, X.; Li, F.; Zhao, Y.; Ma, L.; Du, M. Circularly Polarized Room-Temperature Phosphorescence and Encapsulation Engineering for MOF-based Fluorescent/Phosphorescent White Light-Emitting Devices. *Adv. Optical Mater.* **2020**, *8*, 2000330. [[CrossRef](#)]

12. Rasheed, T.; Nabeel, F. Luminescent Metal–Organic Frameworks as Potential Sensory Materials for Various Environmental Toxic Agents. *Coord. Chem. Rev.* **2019**, *401*, 213065. [[CrossRef](#)]
13. Li, H.; Zhao, S.; Zang, S.; Li, J. Functional Metal–Organic Frameworks as Effective Sensors of Gases and Volatile Compounds. *Chem. Soc. Rev.* **2020**, *49*, 6364–6401. [[CrossRef](#)]
14. Jiang, Y.Y.; Zhang, K.; Zhou, M.S.; Gao, P.F.; Fu, H.R. A Fluorescence/Phosphorescence Dual-Emitting Metal–Organic Framework Exhibiting Two Approaches for Single-Phase White-Light Emission. *J. Solid State Chem.* **2021**, *304*, 122563. [[CrossRef](#)]
15. Liu, J.; Zhao, Y.; Dang, L.; Yang, G.; Ma, L.; Li, D.; Wang, Y. Highly Stable 3D Porous Hmof with Enhanced Catalysis and Fine Color Regulation by The Combination Of d- And p-Ions When Compared with Those of Its Monometallic MOFs. *Chem. Commun.* **2020**, *56*, 8758–8761. [[CrossRef](#)]
16. Tan, Y.; Wang, F.; Zhang, J. Design and Synthesis of Multifunctional Metal–Organic Zeolites. *Chem. Soc. Rev.* **2018**, *47*, 2130–2144. [[CrossRef](#)] [[PubMed](#)]
17. Wu, X.; Fu, H.R.; Han, M.; Zhou, Z.; Ma, L.F. Tetraphenylethylene Immobilized Metal–Organic Frameworks: Highly Sensitive Fluorescent Sensor for the Detection of $\text{Cr}_2\text{O}_7^{2-}$ and Nitroaromatic Explosives. *Cryst. Growth Des.* **2017**, *17*, 6041–6048. [[CrossRef](#)]
18. Liu, X.; Wang, K.; Chang, Z.; Zhang, Y.; Xu, J.; Zhao, Y.S.; Bu, X. Engineering Donor-Acceptor Heterostructure Metal–Organic Framework Crystals for Photonic Logic Computation. *Angew. Chem. Int. Ed.* **2019**, *58*, 13890–13896. [[CrossRef](#)]
19. Leith, G.A.; Martin, C.R.; Mayers, J.M.; Kittikhunnatham, P.; Larsen, R.W.; Shustova, N.B. Confinement-Guided Photophysics in MOFs, COFs, and Cages. *Chem. Soc. Rev.* **2021**, *50*, 4382–4410. [[CrossRef](#)]
20. Cui, Y.; Zhang, J.; He, H.; Qian, G. Photonic Functional Metal–Organic Frameworks. *Chem. Soc. Rev.* **2018**, *47*, 5740–5785. [[CrossRef](#)]
21. Shu, Y.; Ye, Q.; Dai, T.; Xu, Q.; Hu, X. Encapsulation of Luminescent Guests to Construct Luminescent Metal–Organic Frameworks for Chemical Sensing. *ACS Sens.* **2021**, *6*, 641–658. [[CrossRef](#)]
22. Xing, S.; Janiak, C. Design and Properties of Multiple-Emitter Luminescent Metal–Organic Frameworks. *Chem. Commun.* **2020**, *56*, 12290–12306. [[CrossRef](#)] [[PubMed](#)]
23. Ma, L.; Yang, J.; Lu, B.; Li, C.; Ma, J. Water-Stable Metal–Organic Framework for Effective and Selective $\text{Cr}_2\text{O}_7^{2-}$ Capture through Single-Crystal to Single-Crystal Anion Exchange. *Inorg. Chem.* **2018**, *57*, 11746–11752. [[CrossRef](#)]
24. Sun, Y.; Wang, F.; Zhang, J. Synthesis of Anionic Metal–Organic Zeolites for Selective Gas Adsorption and Ion Exchange. *Inorg. Chem.* **2019**, *58*, 4076–4079. [[CrossRef](#)] [[PubMed](#)]
25. Zhao, X.; Yu, X.; Wang, X.; Lai, S.; Sun, Y.; Yang, D. Recent Advances in Metal–Organic Frameworks for the Removal of Heavy Metal Oxoanions From Water. *Chem. Eng. J.* **2021**, *407*, 127221. [[CrossRef](#)]
26. Kobielska, P.; Howarth, A.J.; Farha, O.K.; Nayak, S. Metal–Organic Frameworks for Heavy Metal Removal from Water. *Coord. Chem. Rev.* **2018**, *358*, 92–107. [[CrossRef](#)]
27. Manna, B.; Desai, A.V.; Kumar, N.; Karmakar, A.; Ghosh, S.K. Single-Crystal-To-Single-Crystal Transformation of An Anion Exchangeable Dynamic Metal–Organic Framework. *CrystEngComm* **2015**, *17*, 8796–8800. [[CrossRef](#)]
28. Lv, X.X.; Shi, L.L.; Li, K.; Li, B.L.; Li, H.Y. An Unusual Porous Cationic Metal–Organic Framework Based On a Tetranuclear Hydroxyl-Copper(I) Cluster For Fast And Highly Efficient Dichromate Trapping Through a Single-Crystal To Single-Crystal Process. *Chem. Commun.* **2017**, *53*, 1860–1863. [[CrossRef](#)] [[PubMed](#)]
29. Li, X.; Xu, H.; Kong, F.; Wang, R. A Cationic Metal–Organic Framework Consisting of Nanoscale Cages: Capture, Separation, and Luminescent Probing of $\text{Cr}_2\text{O}_7^{2-}$ through a Single-Crystal to Single-Crystal Process. *Angew. Chem. Int. Ed.* **2013**, *52*, 13769–1377326. [[CrossRef](#)]
30. Ye, C.; Zhou, L.; Wang, X.; Liang, Z. Photon Upconversion: From Two-Photon Absorption (TPA) to Triplet–Triplet Annihilation (TTA). *Phys. Chem. Chem. Phys.* **2016**, *18*, 10818–10835. [[CrossRef](#)]
31. He, Y.; Tan, Y.; Zhang, J. Functional Metal–Organic Frameworks Constructed from Triphenylamine-based Polycarboxylate Ligands. *Coord. Chem. Rev.* **2018**, *420*, 213354. [[CrossRef](#)]
32. Summers, G.H.; Lefebvre, J.; Black, F.A.; Davies, E.S.; Gibson, E.A.; Pullerits, T.; Wood, C.J.; Zidek, K. Design And Characterisation of Bodipy Sensitizers for Dye-Sensitized NiO Solar Cells. *Phys. Chem. Chem. Phys.* **2016**, *18*, 1059–1070. [[CrossRef](#)] [[PubMed](#)]
33. Yang, G.; Liao, Y.; Su, Z.; Zhang, H.; Wang, Y. Theoretical Study on Photophysical and Charge Transport Properties of 1,6-Bis(2-hydroxyphenol)pyridylboron Bis(4-n-butylphenyl)phenyleneamine Compound. *J. Phys. Chem. A* **2006**, *110*, 8758–8762. [[CrossRef](#)] [[PubMed](#)]
34. Gu, Z.; Zhan, C.; Zhang, J.; Bu, X. Chiral Chemistry Of Metal–Camphorate Frameworks. *Chem. Soc. Rev.* **2016**, *45*, 3122–3144. [[CrossRef](#)]
35. Bai, Y.; Dou, Y.; Xie, L.; Rutledge, W.; Li, J.; Zhou, H. Zr-based Metal–Organic Frameworks: Design, Synthesis, Structure, and Applications. *Chem. Soc. Rev.* **2016**, *45*, 2327–2367. [[CrossRef](#)]
36. Zhao, Y.; Wang, Y.; Wang, N.; Zheng, P.; Fu, H.; Han, M.; Ma, L.; Wang, L. Tetraphenylethylene-Decorated Metal–Organic Frameworks as Energy-Transfer Platform for the Detection of Nitro-Antibiotics and White-Light Emission. *Inorg. Chem.* **2019**, *58*, 12700–12706. [[CrossRef](#)]
37. Liu, J.; Yang, G.; Jin, J.; Wu, D.; Ma, L.; Wang, Y. A First New Porous d-p HMOF Material with Multiple Active Sites for Excellent CO_2 Capture and Catalysis. *Chem. Commun.* **2020**, *56*, 2395–2398. [[CrossRef](#)]
38. Eddaoudi, M.; Sava, D.F.; Eubank, J.F.; Adil, K.; Guillerm, V. Zeolite-Like Metal–Organic Frameworks (ZMOFs): Design, Synthesis, and Properties. *Chem. Soc. Rev.* **2015**, *44*, 228–249. [[CrossRef](#)]

39. Zhao, Y.; Wang, L.; Fan, N.; Han, M.; Yang, G.; Ma, L. Porous Zn(II)-Based Metal–Organic Frameworks Decorated with Carboxylate Groups Exhibiting High Gas Adsorption and Separation of Organic Dyes. *Cryst. Growth Des.* **2018**, *18*, 7114–7121. [[CrossRef](#)]
40. Yao, X.; Cao, D.; Hu, J.; Li, Y.; Guo, Z.; Zheng, H. Chiral and Porous Coordination Polymers Based on an N-Centered Triangular Rigid Ligand. *Cryst. Growth Des.* **2011**, *11*, 231–239. [[CrossRef](#)]
41. Wu, H.; Yang, J.; Liu, Y.; Ma, J. pH-Controlled Assembly of Two Unusual Entangled Motifs Based on a Tridentate Ligand and Octamolybdate Clusters: $1D + 1D \rightarrow 3D$ Poly-Pseudorotaxane and $2D \rightarrow 2D \rightarrow 3D$ Polycatenation. *Cryst. Growth Des.* **2012**, *12*, 2272–2276. [[CrossRef](#)]
42. Wu, H.; Yang, J.; Su, Z.; Batten, S.R.; Ma, J. An Exceptional 54-Fold Interpenetrated Coordination Polymer with 10(3)-Srs Network Topology. *J. Am. Chem. Soc.* **2011**, *133*, 11406–11409. [[CrossRef](#)] [[PubMed](#)]
43. Wu, H.; Liu, H.; Yang, J.; Liu, B.; Ma, J.; Liu, Y.; Liu, Y. Series of Coordination Polymers based on Different Carboxylates and a Tri(4-imidazolylphenyl)amine Ligand: Entangled Structures and Photoluminescence. *Cryst. Growth Des.* **2011**, *11*, 2317–2324. [[CrossRef](#)]
44. Yao, X.; Zhang, M.; Hu, J.; Li, Y.; Guo, Z.; Zheng, H. Two Porous Zinc Coordination Polymers with (10,3) Topological Features Based on a N-Centered Tripodal Ligand and the Conversion of a (10,3)-d Subnet to a (10,3)-a Subnet. Chiral and Noncentrosymmetric Metal–Organic Frameworks Featuring A $2D \rightarrow 3D$ Parallel/Parallel Inclined Subpolycatenation. *Cryst. Growth Des.* **2011**, *11*, 3039–3044.
45. Yao, X.; Hu, J.; Zhang, M.; Qin, L.; Li, Y.; Guo, Z.; Zheng, H. Chiral and Noncentrosymmetric Metal–Organic Frameworks Featuring a $2D \rightarrow 3D$ Parallel/Parallel Inclined Subpolycatenation. *Cryst. Growth Des.* **2013**, *13*, 3381–3388. [[CrossRef](#)]
46. Zhang, M.; Di, C.; Qin, L.; Yao, X.; Li, Y.; Guo, Z.; Zheng, H. Diverse Structures of Metal–Organic Frameworks Based on a New Star-Like Tri(4-pyridylphenyl)amine Ligand. *Cryst. Growth Des.* **2012**, *12*, 3957–3963. [[CrossRef](#)]
47. Zhang, M.; Zheng, H.; Lu, Z.; Yao, X. Application of W–Cu–S-based Secondary Building Units in Functional Metal–Organic Frameworks. *CrystEngComm* **2013**, *15*, 9265–9275. [[CrossRef](#)]
48. Shen, K.; Zhang, M.; Zheng, H. Critical Factors Influencing the Structures and Properties of Metal–Organic Frameworks. *CrystEngComm* **2015**, *17*, 981–991. [[CrossRef](#)]
49. Meng, F.; Qin, L.; Zhang, M.; Zheng, H. Two Pairs Of Isomorphism and Two 3D Metal–Organic Frameworks based on a Star-Like Ligand Tri(4-Pyridylphenyl)Amine. *CrystEngComm* **2014**, *16*, 698–706. [[CrossRef](#)]
50. Meng, F.; Zhang, M.; Shen, K.; Li, Y.; Zheng, H. A series of MOFs based on a Triangular Tri(4-Pyridylphenyl)Amine Ligand Combined With Carboxylate Or Nitrate Auxiliary Ligands. *Dalton Trans.* **2015**, *44*, 1412–1419. [[CrossRef](#)]
51. Zhang, M.; Shi, Z.; Chen, M.; Zheng, H. Chiral Crystallization and Optical Properties of Three Metal Complexes based on Two Non-Centrosymmetric Tripodal Ligands. *Dalton Trans.* **2015**, *44*, 5818–5825. [[CrossRef](#)]
52. Shi, Z.; Pan, Z.; Zhang, C.; Zheng, H. Syntheses, Structures, and Properties of Six Cobalt(II) Complexes Based on a Tripodal Tris(4-(1H-1,2,4-Triazol-1-Yl)Phenyl)Amine Ligand. *Dalton Trans.* **2015**, *44*, 16854–16864. [[CrossRef](#)]
53. Wang, Y.; Wang, F. Synthesis, Crystal Structure And Photoluminescence of a Copper(I)-Iodide Coordination Polymer Based On Polyimidazolate Ligand. *Chinese J. Struct. Chem.* **2019**, *38*, 1759–1763.
54. Desai, A.V.; Sharma, S.; Roy, A.; Ghosh, S.K. Probing the Role of Anions in Influencing the Structure, Stability, and Properties in Neutral N-Donor Linker based Metal–Organic Frameworks. *Cryst. Growth Des.* **2019**, *19*, 7046–7054. [[CrossRef](#)]
55. Yao, X.; Xiao, G.; Xie, H.; Qin, D.; Ma, H.; Liu, J.; Yan, P. Two Triphenylamine-Based Luminescent Metal–Organic Frameworks as a Dual-Functional Sensor for the Detection of Nitroaromatic Compounds and Ofloxacin Antibiotic. *CrystEngComm* **2019**, *21*, 2559–2570. [[CrossRef](#)]
56. Yao, X.; Pan, Z.; Hu, J.; Li, Y.; Guo, Z.; Zheng, H. The rational synthesize of (10,3)-type MOFs based on tetraunclear $[W(Mo)OS_3Cu_3]^+$ Secondary Building Units. *Chem. Commun.* **2011**, *47*, 10049–10051. [[CrossRef](#)] [[PubMed](#)]
57. Zhuo, C.; Sun, Y.; Wang, F.; Zhang, J. In Situ Encapsulation of Organic Sulfates in Layered Structures of Zinc and Tris(4-(1H-Imidazol-1-yl)phenyl)amine. *Cryst. Growth Des.* **2020**, *20*, 4228–4231. [[CrossRef](#)]
58. Huo, J.; Li, H.; Yu, D.; Arulsamy, N. Three New Metal Complexes with Imidazole-Containing Tripodal Ligands as Fluorophores for Nitroaromatics- And Ion-Selective Sensing. *Inorg. Chim. Acta* **2020**, *502*, 119310. [[CrossRef](#)]
59. Huo, J.; Yu, D.; Li, H.; Luo, B.; Arulsamy, N. Mechanistic Investigation Of Photocatalytic Degradation Of Organic Dyes by A Novel Zinc Coordination Polymer. *RSC Adv.* **2019**, *9*, 39323–39331. [[CrossRef](#)]
60. Fu, H.R.; Kang, Y.; Zhang, J. Highly Selective Sorption of Small Hydrocarbons and Photocatalytic Properties of Three Metal–Organic Frameworks Based on Tris(4-(1H-imidazol-1-yl)phenyl)amine Ligand. *Inorg. Chem.* **2014**, *53*, 4209–4214. [[CrossRef](#)]
61. Fu, H.R.; Xu, Z.; Zhang, J. Water-stable Metal–Organic Frameworks for Fast and High Dichromate Trapping via Single-Crystal-to-Single-Crystal Ion-exchange. *Chem. Mater.* **2015**, *27*, 205–210. [[CrossRef](#)]
62. Fu, H.R.; Wang, N.; Qin, J.H.; Han, M.L.; Ma, L.F.; Wang, F. Spatial Confinement of A Cationic MOF: A SC-SC Approach for High Capacity Cr(VI)-oxyanion Capture in Aqueous Solution. *Chem. Commun.* **2018**, *54*, 11645–11648. [[CrossRef](#)] [[PubMed](#)]
63. Fu, H.R.; Zhao, Y.; Zhou, Z.; Yang, X.; Ma, L.F. Neutral ligand TIPA-based two 2D Metal–Organic frameworks: Ultrahigh selectivity of C₂H₂/CH₄ and efficient sensing and sorption of Cr(VI). *Dalton Trans.* **2018**, *47*, 3725–3732. [[CrossRef](#)]
64. Desai, A.V.; Manna, B.; Karmakar, A.; Sahu, A.; Ghosh, S.K. A Water-Stable Cationic Metal–Organic Framework as a Dual Adsorbent of Oxoanion Pollutants. *Angew. Chem. Int. Ed.* **2016**, *55*, 7811–7815. [[CrossRef](#)]
65. Jiang, X.; Han, S.; Wang, A.; Pan, J.; Wang, G. The Tri(imidazole)-Derivative Moiety: A New Category of Electron Acceptors for the Design of Crystalline Hybrid Photochromic Materials. *Chem. Eur. J.* **2021**, *27*, 1410–1415. [[CrossRef](#)]

66. Zhuo, C.; Wang, F.; Zhang, J. Mixed Short and Long Ligands toward the Construction of Metal-Organic Frameworks with Large Pore Openings. *Cryst. Growth Des.* **2019**, *19*, 3120–3123. [[CrossRef](#)]
67. Yuan, S.; Deng, Y.; Xuan, W.; Wang, X.; Wang, S.; Dou, J.; Sun, D. Spontaneous Chiral Resolution of a 3D (3,12)-connected MOF with An Unprecedented ttt Topology Consisting of Cubic $[Cd_4(\mu_3-OH)_4]$ Clusters and Propeller-like Ligands. *CrystEngComm* **2014**, *16*, 3829–3833. [[CrossRef](#)]
68. He, Y.; Chen, G.; Yuan, L.; Zhang, L.; Zhang, J. $Ti_4(embonate)_6$ Cage-Ligand Strategy on the Construction of Metal-Organic Frameworks with High Stability and Gas Sorption Properties. *Inorg. Chem.* **2020**, *59*, 964–967. [[CrossRef](#)]
69. Sharma, S.; Desai, A.V.; Joarder, B.; Ghosh, S.K. A Water-Stable Ionic MOF for the Selective Capture of Toxic Oxoanions of Se VI and As V and Crystallographic Insight into the Ion-Exchange Mechanism. *Angew. Chem. Int. Ed.* **2020**, *59*, 7788–7792. [[CrossRef](#)] [[PubMed](#)]
70. Shen, N.; Yang, Z.; Liu, S.; Dai, X.; Xiao, C.; Taylor-Pashow, K.; Li, D.; Yang, C.; Li, J.; Zhang, Y.; et al. $^{99}TcO_4^-$ Removal from Legacy Defense Nuclear Waste by an Alkaline-Stable 2D CationicMetal organic Framework. *Nat. Commun.* **2020**, *11*, 5571. [[CrossRef](#)] [[PubMed](#)]
71. Fu, H.R.; Wu, X.; Ma, L.; Wang, F.; Zhang, J. Dual-Emission SG7@MOF Sensor via SC-SC Transformation: Enhancing the Formation of Excimer Emission and the Range and Sensitivity of Detection. *ACS Appl. Mater. Interfaces* **2018**, *10*, 18012–18020. [[CrossRef](#)]
72. Yuan, S.; Deng, Y.; Sun, D. Unprecedented Second-Timescale Blue/Green Emissions and Iodine-Uptake-Induced Single-Crystal-to-Single-Crystal Transformation in $ZnII/CdII$ Metal-Organic Frameworks. *Chem. Eur. J.* **2014**, *20*, 10093–10098. [[CrossRef](#)]
73. Ge, R.; Li, X.X.; Zheng, S.T. Recent Advances in Polyoxometalate-Templated High-Nuclear Silver Clusters. *Coord. Chem. Rev.* **2020**, *421*, 213787.
74. Jin, Y.; Zhang, C.; Dong, X.; Zang, S.; Mak, T.C.W. Shell Engineering to Achieve Modification and Assembly of Atomically-Precise Silver Clusters. *Chem. Soc. Rev.* **2021**, *50*, 2297–2319. [[CrossRef](#)]
75. Guillerm, V.; Kim, D.; Eubank, J.F.; Luebke, R.; Liu, X.; Adil, K.; Lah, M.S.; Eddaoudi, M. A Supermolecular Building Approach For The Design and Construction Of Metal-Organic Frameworks. *Chem. Soc. Rev.* **2014**, *43*, 6141–6172. [[CrossRef](#)] [[PubMed](#)]
76. Kang, Y.; Wang, F.; Zhang, J.; Bu, X. Luminescent MTN-type Cluster-Organic Framework with 2.6 nm Cages. *J. Am. Chem. Soc.* **2012**, *134*, 17881–17884. [[CrossRef](#)] [[PubMed](#)]
77. Guo, F.; Su, C.; Fan, Y.; Shi, W.; Zhang, X. Assembly of Two Self-Interpenetrating Metal-Organic Frameworks Based on a Trigonal Ligand: Syntheses, Crystal Structures, and Properties. *Inorg. Chem.* **2020**, *59*, 7135–7142. [[CrossRef](#)]
78. Winnik, F.M. Photophysics of Preassociated Pyrenes in Aqueous Polymer Solutions and In Other Organized Media. *Chem. Rev.* **1993**, *93*, 587–614. [[CrossRef](#)]
79. Fu, H.R.; Yan, L.; Wu, N.; Ma, L.; Zang, S. Dual-emission MOF-dye Sensor For Ratiometric Fluorescence Recognition of RDX and Detection Of a Broad Class Of Nitro-Compounds. *J. Mater. Chem. A* **2018**, *6*, 9183–9191. [[CrossRef](#)]
80. Zhai, Q.; Bu, X.; Zhao, X.; Li, D.; Feng, P. Pore Space Partition in Metal-Organic Frameworks. *Acc. Chem. Res.* **2017**, *50*, 407–417. [[CrossRef](#)] [[PubMed](#)]
81. Desaia, A.V.; Sharmaa, S.; Leta, S.; Ghosh, S.K. N-donor Linker Based Metal-Organic Frameworks (Mofs): Advancement and Prospects as Functional Materials. *Coord. Chem. Rev.* **2019**, *395*, 146–192. [[CrossRef](#)]
82. Loukopoulos, E.; Kostakis, G.E. Recent Advances in The Coordination Chemistry of Benzotriazole-Based Ligands. *Coord. Chem. Rev.* **2019**, *395*, 193–229. [[CrossRef](#)]
83. Jeoung, S.; Kim, S.; Kim, M.; Moon, H.R. Pore Engineering Of Metal-Organic Frameworks with Coordinating Functionalities. *Coord. Chem. Rev.* **2020**, *420*, 213377. [[CrossRef](#)]
84. Hu, X.; Wang, Z.; Su, Y.; Chen, P.; Jiang, Y.; Zhang, C.; Wang, C. Metal-Organic Layers with an Enhanced Two-Photon Absorption Cross-Section and Up-Converted Emission. *Chem. Mater.* **2021**, *33*, 1618–1624. [[CrossRef](#)]
85. Hirata, S.; Totani, K.; Zhang, J.; Yamashita, T.; Kaji, H.; Marder, S.R.; Watanabe, T.; Adachi, C. Efficient Persistent Room Temperature Phosphorescence in Organic Amorphous Materials under Ambient Conditions. *Adv. Funct. Mater.* **2013**, *23*, 3386–3397. [[CrossRef](#)]
86. Belyaev, A.; Cheng, Y.; Liu, Z.; Karttunen, A.J.; Chou, P.; Koshevoy, I.O. A Facile Molecular Machine: Optically Triggered Counterion Migration by Charge Transfer of Linear Donor- π -Acceptor Phosphonium Fluorophores. *Angew. Chem. Int. Ed.* **2019**, *58*, 13456–13465. [[CrossRef](#)] [[PubMed](#)]
87. Zhou, Y.; Qin, W.; Du, C.; Gao, H.; Zhu, F.; Liang, G. Long-Lived Room-Temperature Phosphorescence for Visual and Quantitative Detection of Oxygen. *Angew. Chem. Int. Ed.* **2019**, *58*, 12102–12106. [[CrossRef](#)] [[PubMed](#)]
88. Lei, Y.; Dai, W.; Tian, Y.; Yang, J.; Li, P.; Shi, J.; Tong, B.; Cai, Z.; Dong, Y. Revealing Insight into Long-Lived Room-Temperature Phosphorescence of Host-Guest Systems. *J. Phys. Chem. Lett.* **2019**, *10*, 6019–6025. [[CrossRef](#)]
89. Chen, K.C.; Liu, B. Enhancing the Performance of Pure Organic Room-Temperature Phosphorescent Luminophores. *Nat. Commun.* **2019**, *10*, 2111.